GI_Forum 2023, Issue 2
Page: 18 - 31
Full Paper
Corresponding Author:
gulam.mohiuddin@hnee.de
DOI: 10.1553/giscience2023_02_s18

Detection of Urban Expansion using the Indices-Based Built-Up Index Derived from Landsat Imagery in Google Earth Engine

Gulam Mohiuddin[1], Jan-Peter Mund[1] and Kazi Jahidur Rahaman[1]
[1]Eberswalde University for Sustainable Development, Germany

Abstract

Urban expansion, particularly in the global south, has brought numerous environmental consequences which require regular investigation. The current study assessed the growth of built-up areas in the Chbar Ampov district (Phnom Penh, Cambodia) using the Indices-Based Built-Up Index (IBI) derived from Landsat 8 satellite imagery. We applied the IBI method to satellite images from 2013 to 2021 to determine changes in the built-up area over time and their correlation with land surface temperature (LST). The research revealed generally consistent urban expansion (1.68 square kilometres per year) in the study area within the period. Despite minor inconsistencies due to temporary land-use changes and cloud interference, the results support the study's major conclusions. The findings reinforce the necessity of meticulous monitoring and management of urban expansion. Dynamic analysis and practical research methods can contribute to sustainable urban development practices, thus ensuring a balance between human progress and environmental preservation.

Keywords:

urban expansion, built-up area, change detection, remote sensing

1 Introduction

Urbanization is a prevalent trend in today's world. It is projected that by 2050, 68% of the global population will inhabit urban areas, with a particularly high percentage in Asia (UN, 2018). Rapid urban expansion and its impacts on the environment and society have recently gained increased attention (Liu et al., 2022). While urban agglomerations offer economic advantages, they also pose environmental problems, such as air and water quality changes, loss of biodiversity, and the urban heat island (UHI) effect (Molina & Molina, 2004). Moreover, urbanization-induced habitat loss and fragmentation affect species distribution and population structures, particularly in the developing world.

Rapid unplanned urbanization can significantly influence inhabitants' health and wellbeing (Mohamed & Worku, 2019; Patra et al., 2018). Thus, it is essential to monitor urban growth, identifying urbanization patterns and trends over time. Studying the expansion of urban areas,

predominantly characterized by man-made structures or built-up areas, is essential for understanding how land cover changes over time. Insights from urban expansion studies can help to take inform decisions about land use and to promote sustainable urban development, management and planning (Feng et al., 2019; Ban et al., 2015; Schneider et al., 2010).

The terms "urban expansion" and "built-up area expansion" are used synonymously in this study, covering any man-made structure, including bare land and construction zones.

Remote sensing helps the study of changes in built-up areas over time by providing a means to observe and analyse the earth's surface (Liu et al., 2022; Nguyen et al., 2018; Dutta et al., 2015; Sharma et al., 2013). Satellite imagery can provide a synoptic coverage of an area over time, allowing the detection and measuring of changes in built-up areas. Hence, remote sensing (in our case, using the cloud-based remote sensing platform Google Earth Engine (GEE)) can help monitor urban expansion, identify areas of growth or decline, and assess the impact of urban development on the environment. GEE has an extensive archive of satellite imagery and built-in tools for data processing, visualization, and analysis (Walker et al., 2022).

Mapping built-up areas is more straightforward and accurate when land-use indices are used (Rasul et al., 2018; Kumar et al., 2012; Xu, 2008), exploiting the fact that built-up surfaces tend to reflect more in the middle infrared region of the electromagnetic spectrum than in the near-infrared (Aggarwal, 2004). The normalized difference built-up index (NDBI) was introduced to extract built-up areas (Zha et al., 2003). Since then, NDBI has been adopted in many studies (Bouhennache et al., 2019; Zhou et al., 2014; Kumar et al., 2012; He et al., 2010; Xu, 2008) and is now arguably the most widely used index for identifying built-up areas. However, researchers have used different indices to identify spatiotemporal changes in urban growth (Mohamed & Worku, 2019; Li et al., 2018; Nguyen et al., 2018; Dutta et al., 2015; Rahman et al., 2012; Maktav & Erbek, 2005). Despite being a popular approach, spectral techniques based on a simple band ratio considering one particular LULC class have limitations for identifying urban areas. Urban areas consist of various land-cover types, such as concrete, asphalt, trees, grass, water, soil and roof materials, which all have different radiometric properties in remote sensing images. Hence, it is challenging to define a spectral class as "urban". Additionally, some urban land-cover categories are similar to non-urban cover types, making it challenging to use a single index for images of both urban and suburban areas (Barnsley & Barr, 1996; Mesev, 1998). The urban landscape was initially generalized using a V-I-S model (vegetation, impervious surfaces and bare soil) (Ridd, 1995). However, this model did not distinguish bodies of open water, an essential part of an urban ecosystem. Waterbodies were therefore masked out before analysis (Wu & Murray, 2003). The normalized difference water index (NDWI) was introduced to extract waterbodies; the spectral index used green and near-infrared bands (NIR) (McFeeters, 1996). Later, it was argued that typical NDWI includes noise from built-up areas, and a modified version of the index, the MNDWI, was proposed to address this challenge (Xu, 2006). This modified version uses a middle-infrared band (e.g. band 6 in Landsat 8) instead of NIR.

Studies suggest that Land Surface Temperature (LST) is another significant indicator for identifying urban areas. For instance, Weng et al. (2008) explored the spatial distribution of LST across different Land Use and Land Cover (LULC) types. The research revealed that areas with heavy urbanization, covered primarily by impermeable surfaces and having scant vegetation, displayed elevated LST values. Another study, by Amiri et al. (2009), employed Landsat satellite data to delve into the impacts of varying LULC types on LST. Their findings suggested that urban zones marked by high density and dominated by concrete and asphalt surfaces demonstrated higher LST values compared to less densely populated residential zones with abundant green spaces. Such insights underscore the potential of LST as a tool in detecting urban areas.

The Indices-based built-up index (IBI) was introduced to address the difficulty of distinguishing between built-up and non-built-up areas using thematic bands (Xu, 2008). IBI uses three land-cover indices covering the urban ecosystem's basic components – vegetation, water and built-up area. Using the Google Earth Engine platform and Landsat imagery, this study used the IBI to investigate the expansion of urban areas in a peripheral district of the city of Phnom Penh in Cambodia from 2013 to 2021.

2 Study area

Chbar Ampov is a district in southeastern Phnom Penh, Cambodia (Figure 1). It was created in December 2013 from existing communes and is separated from the city by the Bassac River. The district has an area of 86.7 square kilometres and a population of 5,280 (National Institute of Statistics, 2019).

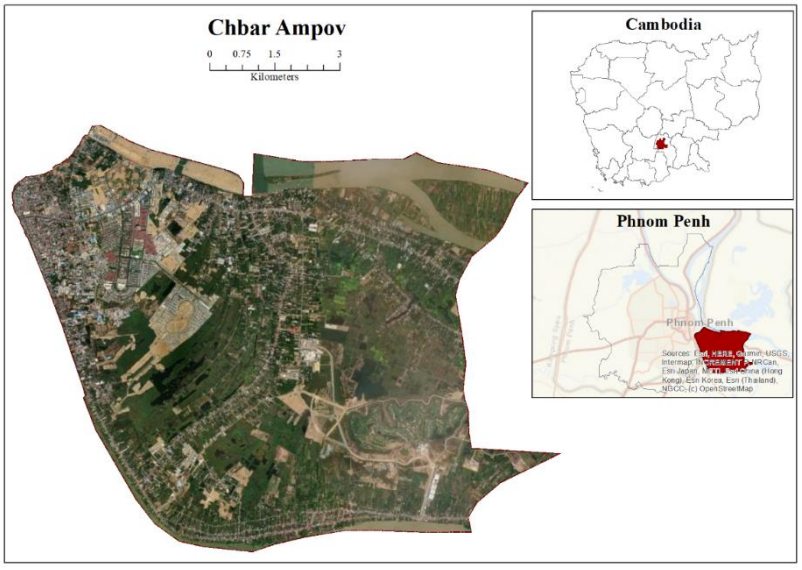

Figure 1: Study area

3 Materials and method

The study used satellite images from the Google Earth Engine Landsat 8 archive. Landsat Tier 1 data were used because they provide the best quality and are particularly suitable for change detection (USGS, 2022). Google Earth historical images were used to interpret the changes in a built-up area and to verify the IBI results.

Applying a cloud filter of 10% generated a total of 30 Landsat-8 images from 2013 to 2021. Before calculating the indices, several pre-processing steps were taken. Cloud-masking was used to remove the cloudy pixels from the analysis. Radiometric calibrations were conducted to correct variations in the sensor's sensitivity to atmospheric conditions over time, and solar illumination at the time of the imaging. All the images were clipped to the study area.

An overview of the complete methodology is given in Figure 2.

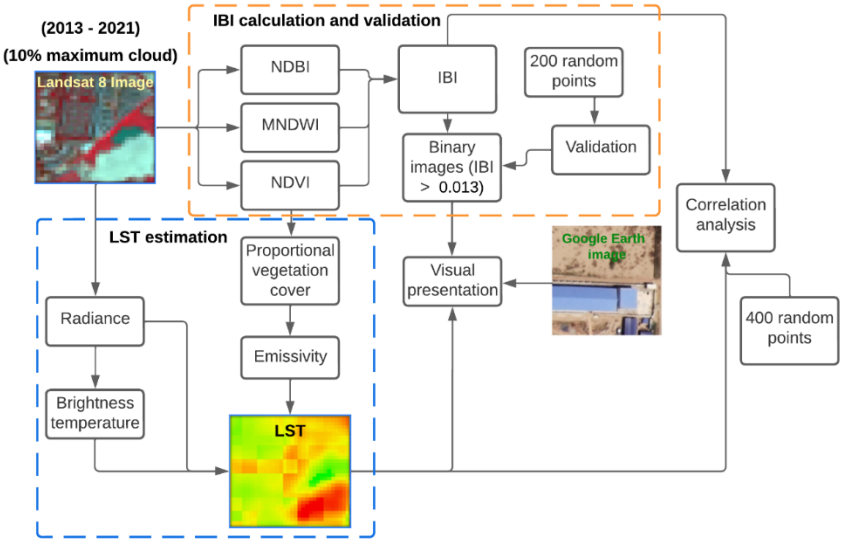

Figure 2: Methodology workflow

3.1 IBI calculation

The indices-based built-up index (IBI) was calculated using three spectral indices: NDBI, MNDWI and normalized difference vegetation index (NDVI) (Equations 1, 2 and 3). Finally, the IBI was calculated by integrating the equations for NDBI, NDVI and MNDWI (Equation 4) (Xu, 2008):

NDBI = (SWIR1 – NIR) / (SWIR1 + NIR) ……...……...(eqn 1)

MNDWI = (G – SWIR1) / (G + SWIR1) ……..……... …(eqn 2)

NDVI = (NIR – R) / (NIR + R) …….....… (eqn 3)

$$IBI = 2 * SWIR1 (SWIR1 + NIR) – [NIR / (NIR + R) + G / (G + SWIR1)] / 2 * SWIR1 (SWIR1 + NIR) + [NIR / (NIR + R) + G / (G + SWIR1)] \quad \ldots \quad (eqn\ 4)$$

where SWIR1 is the first shortwave infrared band, NIR is the near-infrared band, G is the green band, and R is the red band, which are located at bands 6, 5, 3 and 4 in Landsat-8.

3.2 LST calculation

Several studies have employed a range of LST estimations Rajeshwari & Mani (2014)). We calculated the LST using one thermal infrared (TIR) band (band 10) and three operational land imager (OLI) bands (bands 3, 4, 5) from the Landsat 8 satellite. The formulas employed for determining LST were sourced from Avdan & Jovanovska (2016). We excluded TIR band 11 from our computations to circumvent increased calibration uncertainty. Landsat Level-1 products have already undergone geometric correction (Young et al., 2017). We performed radiometric (Equation 5) and thermal calibration (Equation 6) as part of the pre-processing:

$$Radiance = R = ML * Qcal + AL \quad (eqn\ 5)$$

where ML and AL are band-specific multiplicative rescaling factors, and Qcal is the thermal band.

$$Top\text{-}of\text{-}atmosphere\ brightness\ temp. = TB = (K2 / \ln(K1 / R + 1) – 273.15 \quad (eqn\ 6)$$

where TB is the top-of-atmosphere brightness temperature, and K1 and K2 are band-specific thermal conversion constants.

Based on the NDVI (Equation 3), the proportion of vegetation (Equation 7) was calculated to estimate emissivity (Equation 8):

$$Prop.\ of\ vegetation = Pv = ((NDVI – NDVImin)/(NDVImax – NDVImin))^2 \quad (eqn\ 7)$$

$$Emissivity = E = 0.004 * Pv + 0.986 \quad (eqn\ 8)$$

where NDVImin and NDVImax are the minimum and maximum values of NDVI.

The LST was then estimated using the brightness temperature, radiance, Planck's constant, velocity of light and emissivity (Equation 9):

$$LST = TB / [1 + (R * TB/ (h * c/s)) * \ln(E)] \quad (eqn\ 9)$$

where TB is the top-of-atmosphere brightness temperature, R is the wavelength of the emitted radiance, h is Planck's constant, c is the velocity of light, s is the time unit (second), and E is emissivity.

3.3 Method for analysis and interpretation

After the IBI calculation, images were converted into binary images using a 0.013 threshold. This threshold was suggested by Xu (2008) in the study that introduced IBI. All pixel values

greater than 0.013 were considered built-up areas; the rest were non-built-up; areas for both classes were calculated from the numbers of pixels. Using binary images from each year, visual interpretation was then carried out to understand yearly changes. A total of seven images were visually presented and interpreted, one image for each year, except 2015 and 2020. The binary images from 2013 and 2021 were compared with Google Earth Images and their respective LSTs to obtain an overview of the changes. To understand the relationship between built-up area and LST, a correlation test between IBI and LST was performed based on 400 random points in the study area.

3.4 Validation of IBI

Validation was carried out using 200 random points to assess the accuracy of the IBI results (Figure 3). The same points were used for each year of the study period. Using Google Earth historical images to calculate user accuracy, producer accuracy and kappa statistics, the points were then validated if they correctly identified the built-up and non-built-up classes.

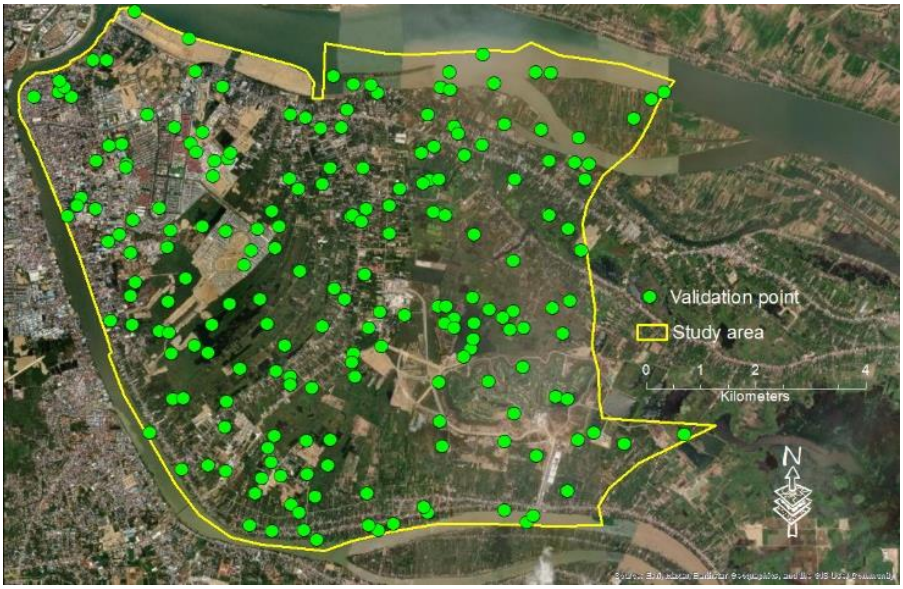

Figure 3: Location of validation points

4 Results

There are visually noticeable changes in the built-up area in Chbar Ampov from 2013 to 2021 (Figure 4) in the northwest and southeast. The northwest part of the district is connected to the core city (Phnom Penh). Changes in this area are part of the urban expansion of the core city, and the change has been gradual.

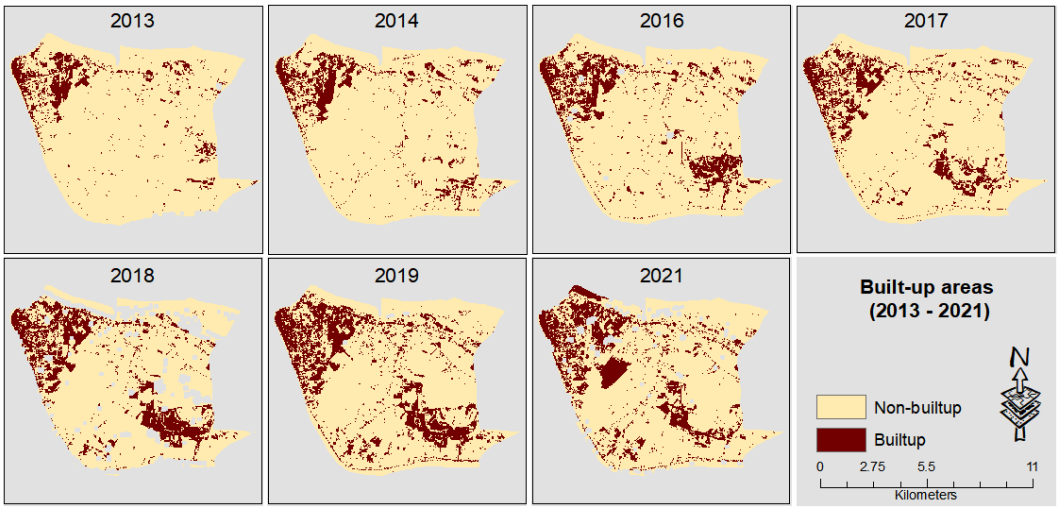

Figure 4: Built-up and non-built-up areas (2013–2021)

The grey patches visible in 2016, 2018, 2019 and 2021 are empty pixels because of cloud. The apparent fluctuations in built-up areas in the southeast are explained below.

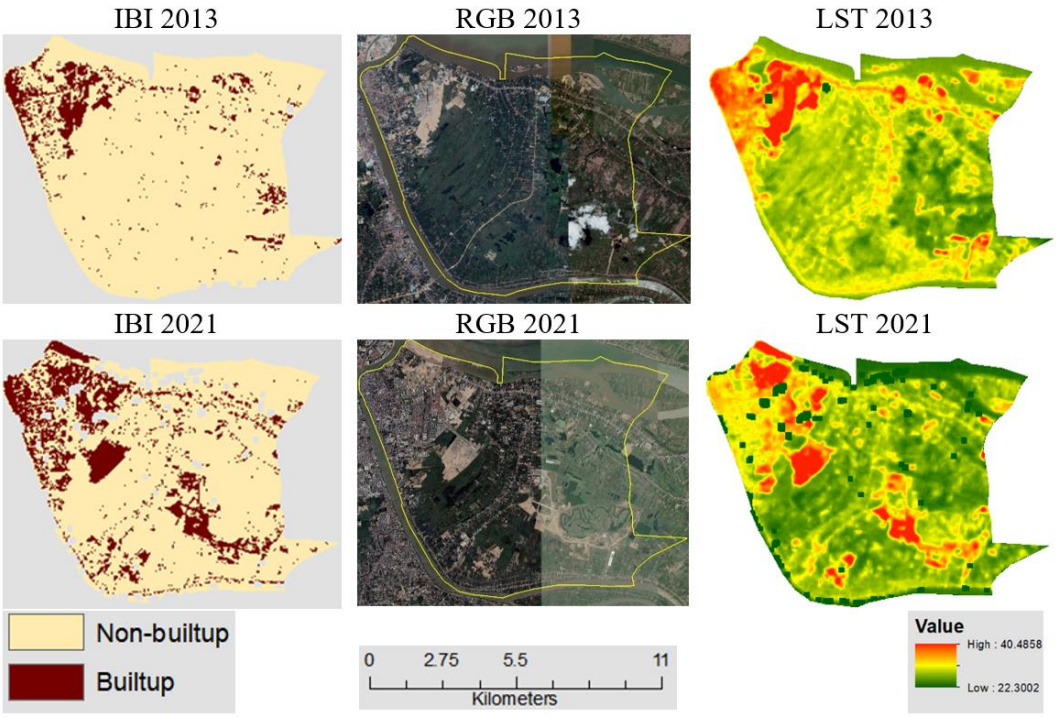

Figure 5: Built-up area changes and LST, 2013 and 2021

Figure 5 illustrates the IBI results, an RGB image (red, green and blue bands) from Google Earth, and LST, for the years 2013 and 2021, allowing the extent of changes to the urban landscape between 2013 to 2021 to be observed directly. By contrast, changes in the southeast are due primarily to the construction of a golf resort. The patterns of built-up areas identified within the IBI correspond visually to those in the Google Earth RGB image and LST.

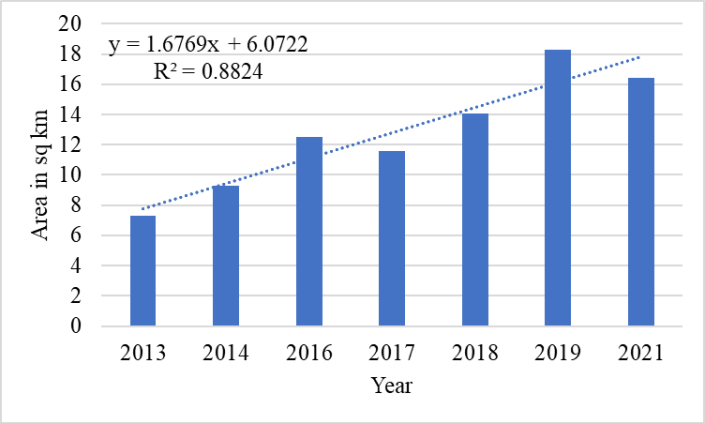

Figure 6: Total built-up area (2013–2021)

The total built-up area is calculated using the number of pixels in each class (presented graphically in Figure 6). The trend line (dotted) suggests a positive relationship between built-up area and time, with an average increase of 1.68 square kilometres per year.

The construction of the golf course in the southeast of the study area in 2016 included bare soil, which was later covered by vegetation. This kind of temporary land use – an area identified as built-up which later becomes non-built-up – explains why some years (2017 and 2021) feature less built-up area than earlier years (2016 and 2019) (see Figure 7 for greater detail). Another reason for differences is cloud cover. For instance, in 2021, areas that in 2020 had appeared as built-up were filtered out because of cloud. It is important to note that the clouds in the Google Earth RGB images are not comparable to the IBI images from Landsat, because the two sets of images do not present the exact same cloud patterns.

Since LST appears to be a useful indicator for identifying built-up areas, a correlation test between IBI and LST was performed at 400 random points. The correlation coefficient was 0.78, indicating a strong correlation between built-up areas and LST (see Figure 8).

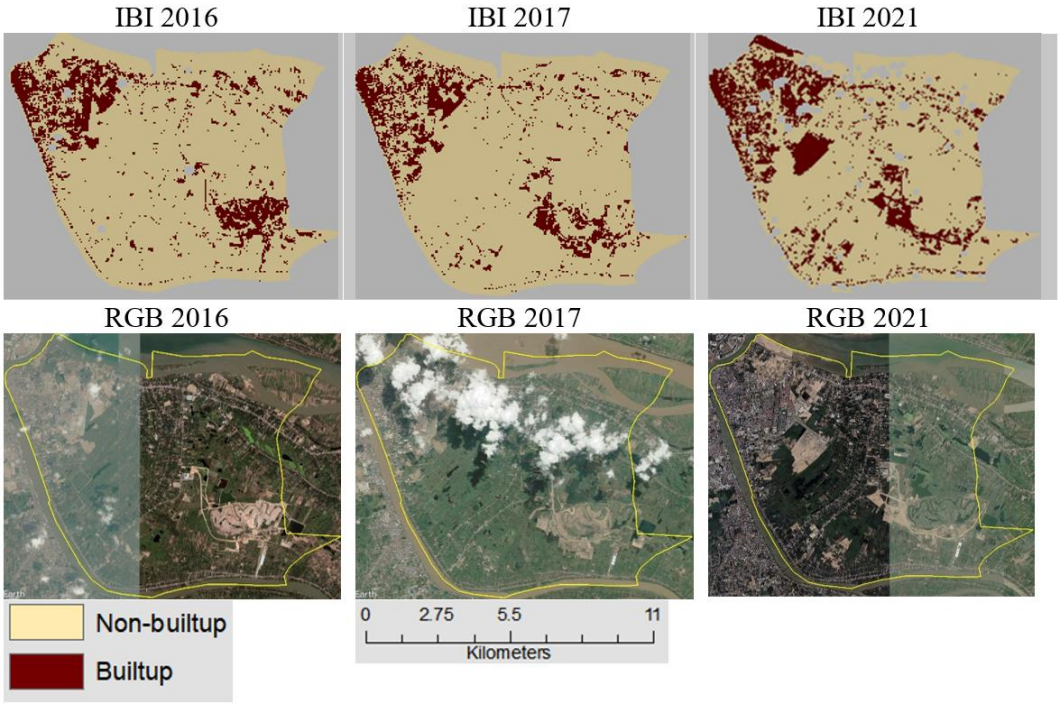

Figure 7: Explanation of the built-up area fluctuation

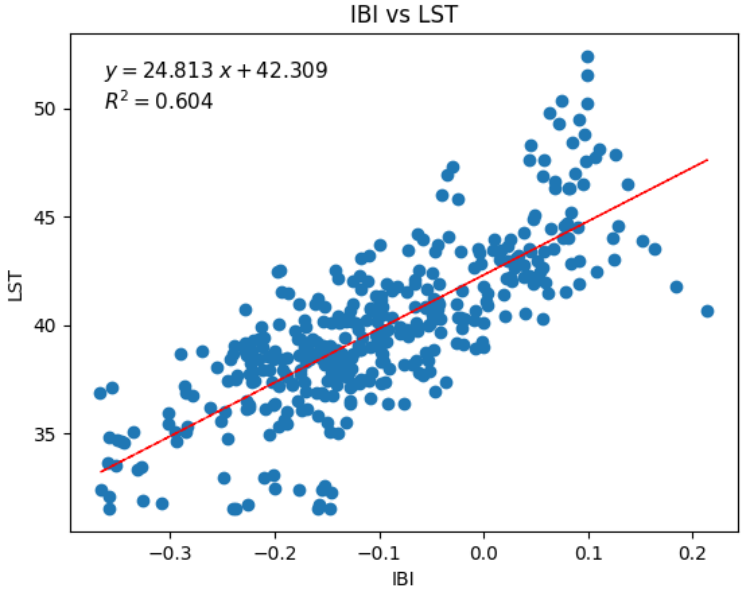

Figure 8: Relationship between IBI and LST

5 Validation of results

A thorough validation of results from the IBI was carried out on 200 random points (Figure 3) using historical images from Google Earth. The producer, user and overall accuracy were calculated to ensure that the IBI results accurately represent the built-up and non-built-up classes. Previous studies stated that the minimum accuracy for classification should be 85% if images are to be interpreted meaningfully (Anderson et al., 1976). Our results showed an overall accuracy of 95 to 98%, and Kappa statistics ranged from 0.85 to 0.88. See Table 1.

Table 1: Accuracy and Kappa statistics of IBI

Year	Overall accuracy	Kappa	Producer accuracy	User accuracy
2013	98.00	0.86	93.33	82.35
2014	98.00	0.88	84.21	94.12
2016	97.00	0.86	95.65	81.48
2017	96.50	0.86	80.65	96.15
2018	96.00	0.87	84.62	94.29
2019	96.00	0.87	85.37	94.59
2021	95.00	0.85	84.78	92.86

6 Discussion

This study evaluated changes in the built-up area in Chbar Ampov between 2013 and 2021 using the IBI derived from Landsat 8 satellite imagery. Our results revealed a generally consistent increase in the built-up area over time, at a rate of approximately 1.68 square kilometres per year. Additionally, the study identified a strong correlation (0.78) between built-up areas and LST, confirming that urban expansion is linked to increased LST.

The built-up area threshold for this study (0.013) was the same as in Xu (2008), where the IBI was first introduced. (Another study used a slightly different threshold (0.018) (Shahfahad et al., 2021).) The threshold value must be selected carefully to ensure that the desired class is within the threshold.

Our findings align with previous research that utilized satellite imagery for urban change detection. For example, various studies reported positive correlations between urbanization and increased land surface temperatures (Zhou et al., 2014; Yang et al., 2014).

While this study provides significant insights into urban expansion, it has some limitations. Firstly, cloud interference is a noticeable issue when the study area is tropical. In the case of Phnom Penh, obtaining cloud-free images is challenging. This study used a 10% maximum cloud filter to shortlist images, but some parts of the study area were cloudy in different

years. This cloud interference affects the calculation of the changes in built-up and non-built-up areas, but as the interference is random and uncertain, it is difficult to address in the calculation. However, since most of the images used in our study have comparatively few cloudy areas, the area calculation is relatively unaffected.

Secondly, land-use changes that turn out to be temporary and the omission of areas in calculation due to cloudy pixels could explain variations observed in the built-up area over time. For instance, the golf course under construction in 2016 was identified as a built-up area, but later parts of it were reclassified as areas of vegetation or water. Such factors affect the estimated expansion rate of built-up areas; they also create inconsistency in a time series.

This study's findings underscore the vital role of satellite imagery in monitoring urban expansion. Urban planners can utilize these insights to optimize city development plans and implement strategies for mitigating urban heat island (UHI) effects. The results also support the theory of UHIs, where urbanization leads to increased LSTs. This increase in LST is due primarily to replacing natural surfaces with built-up areas, which absorb and re-radiate more heat (Oke, 1982).

A more extended time series for the whole city of Phnom Penh, including a buffer area around the city, would be helpful for a holistic picture of the city's urban expansion. To address the problem of cloud interference, a fusion between radar and multispectral images would help in obtaining uninterrupted time series data, since radar data are not affected by cloud (Reiche et al., 2015) and built-up areas return stronger radar signals. Visualizations of LST and built-up areas can be compared in order to understand UHIs more fully. Machine learning and deep learning-based supervised classification are effective methods to extract different LULC classes. They could offer a fruitful approach to build time series for future studies (Li et al., 2019). Finally, the relationship between urban expansion and other environmental parameters like air quality or vegetation cover can be investigated using our approach.

7 Conclusion

The intensifying phenomenon of urban expansion and its environmental impacts, especially in the global south, necessitate the continuous monitoring of urban growth. This study offers insights into urban change detection utilizing the IBI derived from Landsat 8 imagery. In the process, it reveals a substantial correlation between the rise in built-up area and LST. While temporary land-use changes and fluctuating weather conditions created an element of inconsistency, the primary deductions of the study remain valid. Furthermore, the methodology used in the study can be applied to other areas and timelines.

In conclusion, this research emphasizes that careful monitoring and managing urban expansion is paramount in the contemporary world, where urbanization is an ever-present reality. Our approach contributes to sustainable urban development through effective

research methods and rigorous analysis, thus helping to ensure a balance between human progress and environmental preservation.

References

Aggarwal, S. (2004). Principles of remote sensing. *Satellite remote sensing and GIS applications in agricultural meteorology*, *23*(2), 23-28.

Amiri, R., Weng, Q., Alimohammadi, A., & Alavipanah, S. K. (2009). Spatial–temporal dynamics of land surface temperature in relation to fractional vegetation cover and land use/cover in the Tabriz urban area, Iran. *Remote sensing of environment*, *113*(12), 2606-2617.

Anderson, J. R. (1976). *A land use and land cover classification system for use with remote sensor data* (Vol. 964). US Government Printing Office.

Avdan, U., & Jovanovska, G. (2016). Algorithm for automated mapping of land surface temperature using LANDSAT 8 satellite data. *Journal of sensors*, *2016*, 1-8.

Ban, Y., Jacob, A., & Gamba, P. (2015). Spaceborne SAR data for global urban mapping at 30 m resolution using a robust urban extractor. *ISPRS Journal of Photogrammetry and Remote Sensing*, *103*, 28-37.

Barnsley, M. J., & Barr, S. L. (1996). Inferring urban land use from satellite sensor images using kernel-based spatial reclassification. *Photogrammetric engineering and remote sensing*, *62*(8), 949-958.

Bouhennache, R., Bouden, T., Taleb-Ahmed, A., & Cheddad, A. (2019). A new spectral index for the extraction of built-up land features from Landsat 8 satellite imagery. *Geocarto International*, *34*(14), 1531-1551.

Dutta, D., Rahman, A., & Kundu, A. (2015). Growth of Dehradun city: An application of linear spectral unmixing (LSU) technique using multi-temporal landsat satellite data sets. *Remote Sensing Applications: Society and Environment*, *1*, 98-111.

Feng, Y., Wang, X., Du, W., Liu, J., & Li, Y. (2019). Spatiotemporal characteristics and driving forces of urban sprawl in China during 2003–2017. *Journal of Cleaner Production*, *241*, 118061.

He, C., Shi, P., Xie, D., & Zhao, Y. (2010). Improving the normalized difference built-up index to map urban built-up areas using a semiautomatic segmentation approach. *Remote Sensing Letters*, *1*(4), 213-221.

Kumar, A., Pandey, A. C., & Jeyaseelan, A. T. (2012). Built-up and vegetation extraction and density mapping using WorldView-II. *Geocarto international*, *27*(7), 557-568.

Li, W., Liu, H., Wang, Y., Li, Z., Jia, Y., & Gui, G. (2019). Deep learning-based classification methods for remote sensing images in urban built-up areas. *IEEE Access*, *7*, 36274-36284.

Li, X., Zhou, Y., Zhu, Z., Liang, L., Yu, B., & Cao, W. (2018). Mapping annual urban dynamics (1985–2015) using time series of Landsat data. *Remote Sensing of Environment*, *216*, 674-683.

Liu, G., Li, J., & Nie, P. (2022). Tracking the history of urban expansion in Guangzhou (China) during 1665–2017: Evidence from historical maps and remote sensing images. *Land Use Policy*, *112*, 105773.

Maktav, D., & Erbek, F. S. (2005). Analysis of urban growth using multi-temporal satellite data in Istanbul, Turkey. *International Journal of Remote Sensing*, *26*(4), 797-810.

McFeeters, S. K. (1996). The use of the Normalized Difference Water Index (NDWI) in the delineation of open water features. *International journal of remote sensing*, *17*(7), 1425-1432.

Mesev, V. (1998). The use of census data in urban image classification. *Photogrammetric engineering and remote sensing*, *64*(5), 431-436.

Mohamed, A., & Worku, H. (2019). Quantification of the land use/land cover dynamics and the degree of urban growth goodness for sustainable urban land use planning in Addis Ababa and the surrounding Oromia special zone. *Journal of Urban Management*, *8*(1), 145-158.

Molina, M. J., & Molina, L. T. (2004). Megacities and atmospheric pollution. *Journal of the Air & Waste Management Association*, *54*(6), 644-680.

National Institute of Statistics. (2019). General Population Census of the Kingdom of Cambodia 2019.

Nguyen, L. H., Nghiem, S. V., & Henebry, G. M. (2018). Expansion of major urban areas in the US Great Plains from 2000 to 2009 using satellite scatterometer data. *Remote Sensing of Environment*, *204*, 524-533.

Oke, T. R. (1982). The energetic basis of the urban heat island. *Quarterly journal of the royal meteorological society*, *108*(455), 1-24.

Patra, S., Sahoo, S., Mishra, P., & Mahapatra, S. C. (2018). Impacts of urbanization on land use/cover changes and its probable implications on local climate and groundwater level. *Journal of urban management*, *7*(2), 70-84.

Rahman, A., Kumar, S., Fazal, S., & Siddiqui, M. A. (2012). Assessment of land use/land cover change in the North-West District of Delhi using remote sensing and GIS techniques. *Journal of the Indian Society of Remote Sensing*, *40*, 689-697.

Rajeshwari, A., & Mani, N. D. (2014). Estimation of land surface temperature of Dindigul district using Landsat 8 data. *International journal of research in engineering and technology*, *3*(5), 122-126.

Rasul, A., Balzter, H., Ibrahim, G. R. F., Hameed, H. M., Wheeler, J., Adamu, B., ... & Najmaddin, P. M. (2018). Applying built-up and bare-soil indices from Landsat 8 to cities in dry climates. *Land*, *7*(3), 81.

Reiche, J., De Bruin, S., Hoekman, D., Verbesselt, J., & Herold, M. (2015). A Bayesian approach to combine Landsat and ALOS PALSAR time series for near real-time deforestation detection. *Remote sensing*, *7*(5), 4973-4996.

Ridd, M. K. (1995). Exploring a VIS (vegetation-impervious surface-soil) model for urban ecosystem analysis through remote sensing: comparative anatomy for cities. *International journal of remote sensing*, *16*(12), 2165-2185.

Schneider, A., Friedl, M. A., & Potere, D. (2010). Mapping global urban areas using MODIS 500-m data: New methods and datasets based on 'urban ecoregions'. *Remote sensing of environment*, *114*(8), 1733-1746.

Sharma, R., Ghosh, A., & Joshi, P. K. (2013). Analysing spatio-temporal footprints of urbanization on environment of Surat city using satellite-derived bio-physical parameters. *Geocarto International*, *28*(5), 420-438.

Shahfahad, Mourya, M., Kumari, B. Tayyab, M., Paarcha, A., Asif, Rahman, A. (2021) Indices based assessment of built-up density and urban expansion of fast growing Surat city using multi-temporal Landsat data sets. *GeoJournal* 86, 1607–1623 (2021).

USGS. (2022). Landsat collection 1. Retrieved January 1, 2023, from https://www.usgs.gov/landsat-missions/landsat-collection-1

UN. (2018). *68% of the world population projected to live in urban areas by 2050, says UN* | UN DESA | United Nations Department of Economic and Social Affairs. Retrieved 11 January 2023, from https://www.un.org/development/desa/en/news/population/2018-revision-of-world-urbanization-prospects.html

Walker, K., Flores-Anderson, A., Villa, L., Griffin, R., Finer, M., & Herndon, K. (2022). An analysis of fire dynamics in and around indigenous territories and protected areas in a Brazilian agricultural frontier. *Environmental Research Letters*, *17*(8), 084030.

Weng, Q., Liu, H., Liang, B., & Lu, D. (2008). The spatial variations of urban land surface temperatures: pertinent factors, zoning effect, and seasonal variability. *IEEE Journal of Selected Topics in Applied Earth Observations and Remote Sensing*, *1*(2), 154-166.

Wu, C., & Murray, A. T. (2003). Estimating impervious surface distribution by spectral mixture analysis. *Remote sensing of Environment*, *84*(4), 493-505.

Xu, H. (2006). Modification of normalised difference water index (NDWI) to enhance open water features in remotely sensed imagery. *International journal of remote sensing*, *27*(14), 3025-3033.

Xu, H. (2008). A new index for delineating built-up land features in satellite imagery. *International journal of remote sensing*, *29*(14), 4269-4276.

Yang, L., Cao, Y., Zhu, X., Zeng, S., Yang, G., He, J., & Yang, X. (2014). Land surface temperature retrieval for arid regions based on Landsat-8 TIRS data: a case study in Shihezi, Northwest China. *Journal of arid land*, *6*, 704-716.

Young, N. E., Anderson, R. S., Chignell, S. M., Vorster, A. G., Lawrence, R., & Evangelista, P. H. (2017). A survival guide to Landsat preprocessing. *Ecology*, *98*(4), 920-932.

Zha, Y., Gao, J., & Ni, S. (2003). Use of normalized difference built-up index in automatically mapping urban areas from TM imagery. *International journal of remote sensing*, *24*(3), 583-594.

Zhou, Y., Yang, G., Wang, S., Wang, L., Wang, F., & Liu, X. (2014). A new index for mapping built-up and bare land areas from Landsat-8 OLI data. *Remote Sensing Letters*, *5*(10), 862-871.